Exact solution of the thermodynamics and size parameters of a polymer confined to a lattice of finite size: Large chain limit

Chad R. Snyder,[1,a)] Charles M. Guttman,[1,b)] and Edmund A. Di Marzio[1,2,c)]
[1]*Materials Science and Engineering Division, National Institute of Standards and Technology (NIST), Gaithersburg, Maryland 20899, USA*
[2]*Bio-Poly-Phase, 14205 Parkvale Road, Rockville, Maryland 20853, USA*

(Received 19 September 2013; accepted 12 December 2013; published online 21 January 2014)

We extend the exact solutions of the Di Marzio-Rubin matrix method for the thermodynamic properties, including chain density, of a linear polymer molecule confined to walk on a lattice of finite size. Our extensions enable (a) the use of higher dimensions (explicit 2D and 3D lattices), (b) lattice boundaries of arbitrary shape, and (c) the flexibility to allow each monomer to have its own energy of attraction for each lattice site. In the case of the large chain limit, we demonstrate how periodic boundary conditions can also be employed to reduce computation time. Advantages to this method include easy definition of chemical and physical structure (or surface roughness) of the lattice and site-specific monomer-specific energetics, and straightforward relatively fast computations. We show the usefulness and ease of implementation of this extension by examining the effect of energy variation along the lattice walls of an infinite rectangular cylinder with the idea of studying the changes in properties caused by chemical inhomogeneities on the surface of the box. Herein, we look particularly at the polymer density profile as a function of temperature in the confined region for very long polymers. One particularly striking result is the shift in the critical condition for adsorption due to surface energy inhomogeneities and the length scale of the inhomogeneities; an observation that could have important implications for polymer chromatography. Our method should have applications to both copolymers and biopolymers of arbitrary molar mass. [http://dx.doi.org/10.1063/1.4857355]

I. INTRODUCTION

Phenomena related to polymers at interfaces and polymers under confinement are scientifically and technologically important (see supplementary material[30] for a brief listing of possible problems). As a result, problems related to polymers at interfaces and under confinement have attracted wide attention by theorists and experimentalists alike. (Some useful recent theoretical work can be found in the papers by Freed *et al.*,[1] Klushin *et al.*,[2] and Muthukumar,[3] and the references therein.) *Exact* treatments, such as the one presented in this paper, can be useful in understanding the underlying physics. Perhaps the earliest exact treatment of the polymer at an attractive interface was the work of Di Marzio and McCracken.[4] It was valid only for the body centered cubic lattice, but it yielded both a true second-order thermodynamic phase transition as well as the notion of a depletion thickness, i.e., dearth of monomers at the surface even if one end is covalently tied to the surface. Results of methods based on a subsequent exact matrix method approaches,[5,6] i.e., the Di Marzio-Rubin formalism, to isolated polymer molecules confined between two parallel walls can tell us two important things. First, the introduction of a polymer-surface interaction leads to exactly solved phase transition phenomena for various lattices,[5,6] and one learns much when a phase transition can be solved exactly. Second, it may be possible to self-consistently extend the treatment that we will develop in this paper, which is also based on the Di Marzio-Rubin formalism, to polymers competing for the same space, since this was done previously and successfully for a polymer confined between parallel walls.[7,8] (A recent review of approaches to treating polymers self-consistently is given by Fredrickson.[9])

One area particularly well served by studies of isolated polymer chains near surfaces is the field of polymer chromatography. Previous matrix[10] and continuum[1] (Gaussian) approaches to various chromatography challenges focused on evaluation of the partition function and enthalpies to look at the adsorption phase transition clearly, since both of these relate to the thermodynamics involved in the chromatography of polymers at the so-called critical point, or critical condition. The chromatographic critical point separates the condition of complete exclusion in the chromatography process to that of complete binding of the polymer by the wall. In the case of complete exclusion, we have size exclusion chromatography (SEC). Here, separation of polymers is viewed as a thermodynamic process in which the chains are partitioned by size into and out of pores.[11–13] In the absorption region, the polymer is separated by the interactions with the walls with the larger polymers lingering longer on the walls. One changes from one process to another by changing temperature (T) or changing interaction energy (solvent mix or solvent quality). In our previous approaches to chromatography using the one-dimensional matrix method, we varied the interaction of the chain with the surface by varying the energy of interaction or temperature of a single chain with the surface,[4,6] and then

[a)]chad.snyder@nist.gov
[b)]charles.guttman@nist.gov
[c)]edmund.dimarzio@nist.gov

changed from a homopolymer to a copolymer and showed the effect of interaction of the different parts of the copolymer with the wall.[10,14] Through the latter approach, it was shown (1) that it is insufficient to model a copolymer as a homopolymer by using some average of the copolymer adsorption energies and (2) that the matrix formalism is useful in predicting the elution behavior of copolymers, e.g., random or block, near the critical condition. In a block copolymer, by using a mixed solvent one can tune out one of the blocks so that it is neutral towards the surface (this happens at its critical point). Then, the remaining block can be eluted out on the basis of its molecular mass only. Some of the more unique predictions regarding the elution behavior of block copolymers have been subsequently validated experimentally.[15]

In this paper, we extend the matrix formalism of the one-dimensional (pseudo 3D) Di Marzio-Rubin model to higher dimensions using Di Marzio-Guttman,[17] with each site on the lattice having its own affinity for each of the individual monomers in the polymer. We note in advance that much of what can be accomplished with the matrix method can also be accomplished with continuum methods; however, continuum models are insensitive to chain structural details. As pointed out by Gorbunov and Skvortsov,[16] continuum methods are more convenient for analysis of global conformational characteristics of molecules; however, they have a "limited 'resolving power', whereas a lattice model permits accounting for the local structure of a macromolecule." Additionally, the matrix method has certain advantages over continuum methods in that it is far easier to define fine-scale boundary conditions such as roughness and energetics. We, therefore, look at the matrix approach as a complementary method to many problems that can be solved using continuum methods.[3] In this paper, we develop the theory that enables local structure analyses and chain length dependent studies, but focus our demonstrations on the limit of freely jointed large chains, to allow qualitative comparisons with the expectations of continuum (Gaussian) methods. As such, we demonstrate the ability of the technique to reproduce well-understood polymer physics phenomena, but show how the technique is capable of changing the fine structure of the boundary conditions to enable examination of far more complex structures. One large advantage to being able to explicitly define non-uniform surface energetics is the ability to examine the effect of varying surface energies, roughness, or combinations of the two along a given surface or regions of space; all three of these combinations are of particular relevance to polymer chromatography. We specifically will examine pseudo three-dimensional (3D) structures, which are infinite rectangular cylinders – the surface walls are defined in terms of the top, bottom, left, and right sides of a rectangle and unrestrained motion is allowed in the third dimension, and we allow variation of the energetics as a function of distance along one wall or on objects contained within the lattice. The effects of chain confinement will be examined as well.

II. THEORETICAL DEVELOPMENT

The core of our method lies in the transition probability matrix **W**. To demonstrate how easily **W** can be set up, we will work with a two-dimensional rectangular lattice of N_x by N_y, where $N_x = 3$ and $N_y = 5$. We use this notation since it will be our notation in the latter part of this paper. As we work through the solution, we will illustrate how these methods can be extended to (1) any dimension, (2) lattices with structure, (3) lattices of any size and of any degree of openness, (4) lattice-site specific energies of attraction of the monomer for the lattice site, and (5) monomer-specific strengths of attraction for the various lattice sites. (Note that items 4 and 5 are different. Item 4 arises because each lattice site has its own energy of attraction for monomers in the transition probability matrix, whereas Item 5 arises because each different monomer in the chain has its own associated matrix.) In the numerical calculations that follow, we will look at a variety of rectangular cylinders, where we allow steps unconstrained in the z direction (pseudo 3D lattice), but the theory is applicable to arbitrary dimensions and lattice types.

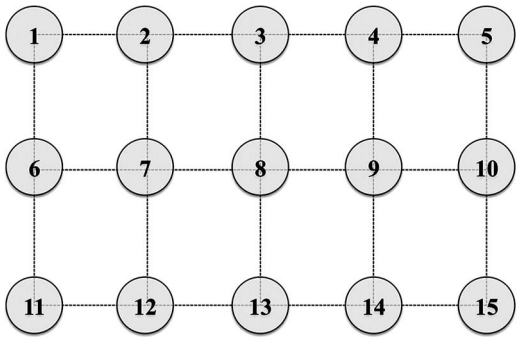

FIG. 1. An example of a square lattice of 3×5 ($N_x \times N_y$) sites. A monomer touching site j will have the weight $w_j = p \exp(-\varepsilon_j/k_BT)$. This allows us to accommodate surface energetics, but it also allows the monomer to have an energy that is a function of position throughout the lattice. Our initial description will be for the case where each monomer has the same energies of attraction for a lattice site as any other, but later we will describe a simple generalization which allows the energy to be monomer specific, that is, to say $w_{j,n} = p \exp(-\varepsilon_{j,n}/k_BT)$, where n is the ordinal location of the nth monomer in a linear chain of N monomers ($1 \le n \le N$) and j is the lattice site number.

In Fig. 1, we label the 15 lattice sites of our 3×5 rectangular lattices from 1 to 15. Now consider the 15×15 transition probability matrix **W** in Fig. 2, which describes the probability of placement of each monomer unit (or "stepping" from one lattice site to another). Each column has the statistical weight of the site represented by the column. For example, column 7 has the weight w_7 but only at those row locations corresponding to its nearest neighbors. For site 7 these locations are 2, 6, 8, and 12. (The extension to explicitly three dimensions would result in a second layer numbered from 16 to 30, etc. Site 7 would then also have a nearest neighbor at location 22.) The weight w_j is given by the Boltzmann exponential:

$$w_j = p \exp(-\varepsilon_j/k_BT), \tag{1}$$

where ε_j is the attractive energy of the lattice site for the polymer segment, k_B is Boltzmann's constant, and p defines the polymer segment's transition probability. For a freely jointed chain, p is typically just the inverse of the lattice coordination number s, i.e., $1/s$. To generalize Eq. (1) to synthetic copolymers or biological polymers, the equation needs to be

	1	2	3	4	5	6	7	8	9	10	11	12	13	14	15
1		w_2				w_6									
2	w_1		w_3				w_7								
3		w_2		w_4				w_8							
4			w_3		w_5				w_9						
5				w_4						w_{10}					
6	w_1						w_7				w_{11}				
7		w_2				w_6		w_8				w_{12}			
8			w_3				w_7		w_9				w_{13}		
9				w_4				w_8		w_{10}				w_{14}	
10					w_5				w_9						w_{15}
11						w_6						w_{12}			
12							w_7				w_{11}		w_{13}		
13								w_8				w_{12}		w_{14}	
14									w_9				w_{13}		w_{15}
15										w_{10}				w_{14}	

FIG. 2. This figure describes the transition probability matrix W used to determine the statistics and thermodynamics of a polymer molecule of N monomers confined to the two-dimensional lattice of Fig. 1. The linear dimension M of the matrix is equal to the number of lattice sites (M = 15). The column labeled j has a weight w_j at every location corresponding to the nearest neighbor sites to site j; the other sites in the column each have the weight zero. The above statements are invariant to the way we label the sites. In the text, it is shown that the partition function (sum over states) is obtained by multiplying the matrix by itself $N-1$ times along with the multiplication by proper fore and aft row and column vectors. (N.B. The matrix to be used for the computations later in this paper will differ from this matrix in shape, in that there will also be non-zero elements on the diagonal describing unconstrained motion in a 3rd dimension. Table I later in this paper elaborates on the differences for different dimensionalities.)

modified such that each monomer unit along the chain can have its own unique affinities for the lattice, i.e.,

$$w_{j,n} = p\exp(-\varepsilon_{j,n}/\mathrm{k_B}T). \tag{2}$$

Here, the subscript j labels the column of the matrix and the subscript n labels the location of the monomer unit in the chain.

If we multiply a column vector with a 1 in position 7 and a zero in the other 14 positions by the matrix (we use the convention row on left multiplies column on right), then we would obtain a new column vector with w_7 at locations 2, 6, 8, and 12. We now multiply this new vector by the matrix again. To envisage what happens it helps to imagine the new column vector to be written as a sum of 4 column vectors, one with zeros everywhere except for a w_7 at location 2, one with w_7 only at location 6, one with w_7 only at location 8, and one with a w_7 only at location 12. Thus, we have, by multiplying the matrix twice, properly accounted for taking two steps starting at location 7, i.e., placing two bonds connecting three monomer units starting with a monomer at location 7. If we multiply by the matrix again we will have counted all of the ways one can have taken three steps, and so on. (See Appendix B for this example in a more detailed matrix form.)

Here, using standard transfer matrix methods, multiplying the starting vector by the matrix $\mathbf{W}$ a total of $N-1$ times corresponds to taking $N-1$ steps on the lattice. To determine the partition function Q (sum over states) for a polymer of N monomer units starting at lattice site k and ending at lattice site j, $\mathbf{W}^{N-1}$ is multiplied from the left by a row vector $\mathbf{P}(..0..w_j..0..)^{\mathrm{T}}$ with w_j at location j and zeros elsewhere and from the right by a column vector $\mathbf{U}_\mathrm{k}$ with 1 at location k and zeros everywhere. Thus, the partition function defined by Q is

$$Q = (\mathbf{P}(..0..w_j..0..))^T\mathbf{W}^{N-1}\mathbf{U}_k \text{ (chain from site } k \text{ to site } j). \tag{3}$$

$(\mathbf{P}(..0..w_j..0..))^T$ is the row vector of Eq. (3) since it is the weight of the last monomer of the polymer chain. The column vector $\mathbf{U}_\mathrm{k}$ can also be thought of as "reading" the probability density at site k. Additionally, if "1" were placed at a number of sites in a vector similar to $\mathbf{U}_\mathrm{k}$, it would provide the combined probability densities from those sites. When serially multiplying the matrices of Eq. (3), the weights carried are from the sites that have been visited while the weight gained is from the site being stepping onto. For copolymers, Eq. (1) is replaced by Eq. (2) and instead of $\mathbf{W}^{N-1}$ in Eq. (3) we have

$$\mathbf{W}^{N-1} \rightarrow \prod \mathbf{W}_n, \tag{4}$$

where $\mathbf{W}_\mathrm{n}$ is the $\mathbf{W}$ matrix with $w_{j,n}$ replacing w_j. Additionally, in the row vector of Eq. (3) w_j is replaced by $w_{j,n}$. Notice that the order of the matrices is now important. This generalization has two uses. First, it can be of use to treat synthetic polymers whose monomers are not all the same, such as random copolymers and block copolymers as was done by Guttman *et al.*[10] It can also be used for the various biological polymers whose monomers are invariably diverse. Second, one can now use the method of Guttman *et al.*[10] to treat star molecules and branched molecules.

For completeness, it should be noted that Q can also be given by the transpose of the right hand side of Eq. (3):

$$Q = (\mathbf{U}_k)^T(\mathbf{W}^T)^{N-1}\mathbf{P}(..0..w_j..0..). \tag{5}$$

The one-dimensional treatment given previously worked with the transpose.[6]

To compute the partition function corresponding to starting anywhere and ending anywhere with an N monomer ($N-1$ step) chain, we sandwich $\mathbf{W}^{N-1}$ with the row vector $\mathbf{P}(0)^{\mathrm{T}}$ on the left and the unity column vector $\mathbf{U} = (1,1,1,..,1,1)$ on the right. Here, we wish to reflect by $\mathbf{P}(0)^{\mathrm{T}}$ the vector which contains w_j at each location j, which corresponds to the probability density vector for placing a single monomer anywhere on the lattice:

$$Q = (\mathbf{P}(0))^{\mathrm{T}}\mathbf{W}^{N-1}\mathbf{U}$$

(chain starting anywhere and ending anywhere). (6)

As an aside, with our approach being an extension of the matrix method to higher dimensions, we need to remark on the difference between linearity and dimensionality. The matrix development of Ref. 6 is linear, but it is not one-dimensional. In fact, the exact solution of the statistics of a single polymer chain between parallel walls that was solved in Ref. 6 is a three-dimensional problem, although the method was limited to uniform surface energetics on smooth surfaces. The method of the present paper is linear in the exact same way as that of Ref. 6, but now enables definition of physical and chemical structure. This linearity emerges from the construction of the polymer molecule one segment at a time. As such, the general formulae of Ref. 6 which depend on matrix algebra are *a fortiori* applicable here as well.

If the matrix **W** in Eq. (3) is diagonalized, then with resulting eigenvalues given by

$$\{\lambda_0, \lambda_1, \lambda_2, \ldots\}, \text{ where } \lambda_0 > \lambda_1 > \lambda_2, \text{etc}, \tag{7}$$

it can be shown that

$$\ln Q \cong \ln[d_0 (\lambda_0)^N + d_1 (\lambda_1)^N + d_2 (\lambda_2)^N + \ldots], \tag{8}$$

where d_i is the degeneracy of the ith eigenvalue. Simplifying yields

$$\begin{aligned} \ln Q &\cong \ln\{\lambda_0{}^N[d_0 + d_1 (\lambda_1/\lambda_0)^N + d_2 (\lambda_2/\lambda_0)^N + \ldots]\} \\ &\cong \ln \lambda_0{}^N + \ln[d_0 + d_1 (\lambda_1/\lambda_0)^N + d_2 (\lambda_2/\lambda_0)^N + \ldots] \end{aligned} \tag{9}$$

and in the limit of large N is simply

$$\ln Q \cong N \ln \lambda_0, \tag{10}$$

which is analogous to the "ground state dominance" approximation used in continuum methods.[3] The connections with thermodynamics are given by the usual formula for the Helmholtz free energy F, entropy S, and energy U:

$$F = -\mathrm{k_B} T \ln Q = U - TS, \quad S = -\partial F/\partial T. \tag{11}$$

In studying polymer/site interactions, a useful quantity is the polymer monomer density as a function of position within the confining walls. For the jth site this is achieved by multiplying each non-zero element of the jth column of the matrix of Fig. 2 by a marker $\exp(\theta_j)$, and then taking the derivative of the transition probability matrix with respect to θ_j in the limit of $\theta_j = 0$. This then returns only those elements of the transition probability matrix that correspond to transitions to site j. (For this method, we have used Eq. (3). If we were using the transpose of Eq. (3) (Eq. (5)), then we would have multiplied the row of the matrix by $\exp(\theta_j)$ as was done in Ref. 6.) The expected number $\langle \nu_j \rangle$ of monomers on site j is then given by the aforementioned derivative divided by the appropriate normalization factor:

$$\langle \nu_j \rangle = \frac{1}{Q} \frac{\partial Q}{\partial \theta_j}\bigg|_{\theta_j=0} = \frac{\partial \ln Q}{\partial \theta_j}\bigg|_{\theta_j=0}. \tag{12}$$

In the case where the first term in Eq. (9) dominates the partition function, the number of segments at any lattice site can also be computed from the eigenvector corresponding to the largest eigenvalue, of the matrix **W**. If the right eigenvector corresponding to the largest eigenvalue λ_0 is

$$\mathbf{r}_0 = (r_{0,1}, r_{0,2}, r_{0,3}, \ldots . r_{0,\mathrm{M}}) \tag{13}$$

and the corresponding left eigenvector is given by

$$\mathbf{l}_0 = (l_{0,1}, l_{0,2}, l_{0,3}, \ldots . l_{0,\mathrm{M}}), \tag{14}$$

then the normalized probability that there is a segment at lattice site m, ρ_m, or the normalized segment density probability, is given by

$$\rho_m = \frac{[(\sum_{i=\text{nearest neighbors to } m} l_{0,i}) + s_0 l_{0,m}] r_{0,m} w_m}{\lambda_0 \mathbf{l}_0 \mathbf{r}_0} \tag{15}$$

as is derived in Appendix A. (The meaning of s_0 will be expanded upon in Sec. III, but it is only relevant to cases where we allow unconstrained motion in a higher dimension.) This form makes intuitive sense. The right eigenvector describes building the chain up from one end to site m, and the left eigenvector describes the chain being built from its opposite end to sites that are nearest neighbors to site m, thus making a complete chain at site m. This also suggests that the density of the joining segment in a block copolymer could be examined using the left and right eigenvectors for each of the blocks in an AB block copolymer, respectively. To make the density computation clearer, we refer to the two-dimensional lattice and corresponding matrix of Figs. 1 and 2, respectively, and provide three examples of how to compute the numerator in Eq. (15):

at the corner (lattice site 1) $= (l_{0,2} + l_{0,6}) r_{0,1} w_1$,
the wall (lattice site 2) $= (l_{0,1} + l_{0,3} + l_{0,7}) r_{0,2} w_2$, and
and in the "bulk" (lattice site 7) $= (l_{0,2} + l_{0,6} + l_{0,8} + l_{0,12}) r_{0,7} w_7$.

These results are exact and can account for many types of interactions but cannot take global excluded volume into account. The effect of *local* excluded volume, i.e., prohibiting immediate step reversal, and local bond structure can be put into the matrix formalism using a sub-matrix approach as described in Sec. V of the Di Marzio-Rubin paper, at the cost of an enlarged matrix.[6]

III. COMPUTATION POSSIBILITIES AND METHODS

Computationally, the method falls into two main stages. First, we produce the matrix **W** that describes the problem. Second, we use matrix algebra to obtain the partition function Q from which the various thermodynamic quantities can be derived. The latter stage also allows calculation of polymer density.

A. Transition probability matrix

In this paper, our calculations will focus on the simple cubic lattice. It is useful to work in the context of Table I.

The matrix describing a walk within the 2D lattice of Fig. 1 is that of Fig. 2 (Dimension = 2D in Table I). As shown in Table I, if the zeroes in the jth element of the diagonal of Fig. 2 are replaced by $2w_j$, walks perpendicular to the plane of the 2D lattice are allowed (Dimension = 2D to pseudo-3D). The factor of 2 arises because each time we step along the z-axis, we can step in the plus or minus z direction. The only requirement is that the energy of these sites be given by $w_j(x, y, z) = w_j(x, y, 0)$, i.e., there are no z-dependent energetics; the x and y energetics project infinitely in the plus and minus z directions. (At this point, the meaning of s_0, introduced in Eq. (15), can be made clear. It is simply equal to the number of lattice directions that are unconstrained. For the case of "2D to pseudo-3D," $s_0 = 2$, as we allow unconstrained movement in the plus and minus z directions. For lattices that do not allow unconstrained motion in some dimension $s_0 = 0$. The entries in the column labeled "Diagonal elements" of Table I could thus all be written as $s_0 w_j$.) The case of

TABLE I. Six separate problems for a polymer walking on a cubic lattice are listed above. The dimensions of the cubic lattice along the x, y, and z orientations are, respectively, a, b, and c; that of the square lattice are a and b; that of the one-dimensional lattice is a. The work of Ref. 6 corresponds to "1D to pseudo-3D" but the present work is more general in that the monomer site interaction energy for the lattice can be an arbitrary function of x. In the case of "1D to pseudo-3D," the meaning of the x, y, z dependence of w_j, $w_j(x, y, z) = w_j(x, 0, 0)$ is that the energetics are defined only in the x direction and hence are extended infinitely in the plus and minus y and z directions. The work of our arxiv.org paper[17] solves the 2D problem and allows for generalization to any dimension. The other 4 problems are simple elaborations of these two solved problems. A similar table can be written for the face centered and body centered lattices. Although we are working here with line and plane boundaries, the method works equally well for other boundaries - arbitrary cylindrical boundaries, for example.

Dimension	Matrix size	Off-diagonal elements	Diagonal elements	Describes	x, y, z dependence of w_j
1D	$a \times a$	w_j	0	Walk on a line	$w_j(x) = w_j(x)$
1D to pseudo-2D	$a \times a$	w_j	$2w_j$	Walk on a plane	$w_j(x, y) = w_j(x, 0)$
1D to pseudo-3D	$a \times a$	w_j	$4w_j$	Walk in 3d	$w_j(x, y, z) = w_j(x, 0, 0)$
2D	$ab \times ab$	w_j	0	Walk in 2d	$w_j(x, y) = w_j(x, y)$
2D to pseudo-3D	$ab \times ab$	w_j	$2w_j$	Walk in 3d	$w_j(x, y, z) = w_j(x, y, 0)$
3D	$abc \times abc$	w_j	0	Walk in 3d	$w_j(x, y, z) = w_j(x, y, z)$

"2D to pseudo-3D" is useful if we wish to examine the statistics and thermodynamics of a polymer molecule in an infinite cylinder. In Sec. IV, we shall calculate and display figures for such infinite rectangular cylinders. Note especially that structure can be easily added into the lattice by preventing certain transitions, i.e., by setting the w_j for various sites equal to zero (swiss cheese-like structures could be created this way).

B. Computational methods

The above formulation of the confined polymer problem will be of value only if the matrices can be handled successfully on the computer. A cube of 30 lattice sites on a side means we are dealing with a large sparse matrix of linear dimension $30 \times 30 \times 30 = 27\,000$, which at $27\,000 \times 27\,000$ would amount to 729 000 000 matrix elements. Even the rectangular cylinder problem would involve a matrix of linear dimension $30 \times 30 = 900$ so the matrix would be 900×900. Thus, it is clear that progress can be made only if we can treat these sparse matrices conveniently. This was done using several readily available open source sparse matrix packages in Fortran95: Sparsekit[18,19] for matrix manipulation and multiplication, and ARPACK[20,21] (ARnoldi PACKage) for solution of eigenvalues and eigenvectors via an implicitly restarted Arnoldi method.[22] (Appropriate matched pairs of left and right eigenvectors for degenerate eigenvalues were identified as those vectors that produced the absolute maximum dot product.) A multithread optimized version of BLAS[23] (Basic Linear Algebra Subprograms) was invoked by ARPACK enabling more rapid computation. The Sparsekit matrix methods were modified to enabling parallelization using OpenMP. Derivatives, when needed, were computed using a Savitzky-Golay algorithm.[24] Density probability contour plots were generated automatically using PLplot.[25] Using compressed matrix storage, in particular, the compressed sparse row (CSR) format, reduced the initial $30 \times 30 \times 30$s matrix elements from 729 000 000 down to a more manageable size of fewer than 351 001 elements [2 arrays of length *less than* (6 diagonals)(27 000 elements each) + one array of length 27 001].

C. Application of computational methods

Using the methods described above, we examine a few simple examples of a chain confined to an infinite rectangular cylinder (simple cubic lattice, lattice coordination number $s = 6$): (1) uniform energetics ($-\varepsilon/k_BT$) on a single wall, (2) uniform energetics ($-\varepsilon/k_BT$) on opposite walls, (3) uniform energetics ($-\varepsilon/k_BT$) on adjacent walls, (4) uniform energetics ($-\varepsilon/k_BT$) on all four walls, (5) alternating energetics every two lattice sites ($-\varepsilon/k_BT$ vs. $-(0.6)\varepsilon/k_BT$) on a single wall, and (6) neutral walls ($-\varepsilon/k_BT = 0$) on the lattice but an object in the center with uniform energetics ($-\varepsilon/k_BT$) on its surface (see Fig. 3). All other walls, and all other lattice sites, have neutral energetics ($-\varepsilon/k_BT = 0$). We allow for unrestrained motion in the z-direction (2D to pseudo 3D, $s_0 = 2$), and the bulk of the lattice has no specific affinities ($-\varepsilon/k_BT = 0$). The weighting factors (w_j) are given by Eq. (1) with $p = s_0/s$ ($p = 2/6$) and $p = 1/s$ ($p = 1/6$) for the diagonal and off-diagonals, respectively, and using the energetics defined above.

Because, in the cases studied here, we limit the ($-\varepsilon/k_BT$) dependence to the walls, it can also be used as a marker variable. Previously, we used the fact that $d[A \exp(\theta)]/d\theta = A \exp(\theta)$ to show how θ could be used to "mark" certain lattice sites or combinations of sites to compute their monomer density (with $\theta = 0$). However, since the energies are limited to the surfaces, $\theta = -\varepsilon/k_BT$, and thus (without setting $\theta = 0$) Eqs. (8) and (12) can be combined to write the fraction of segments on the surface as

$$\frac{\langle v_s \rangle}{N} = \lim_{N\to\infty}\left(\frac{1}{N}\right)\frac{\partial \ln Q}{\partial(\varepsilon/k_BT)}$$

$$= \lim_{N\to\infty}\left(\frac{1}{N}\right)\frac{\partial \ln\left\{\lambda_0^N\left[1 + \frac{d_1}{d_0}\left(\frac{\lambda_1}{\lambda_0}\right)^N + \ldots\right]\right\}}{\partial(\varepsilon/k_BT)}.$$

$$= \left(\frac{1}{\lambda_0}\right)\frac{\partial\lambda_0}{\partial(\varepsilon/k_BT)}. \quad (16)$$

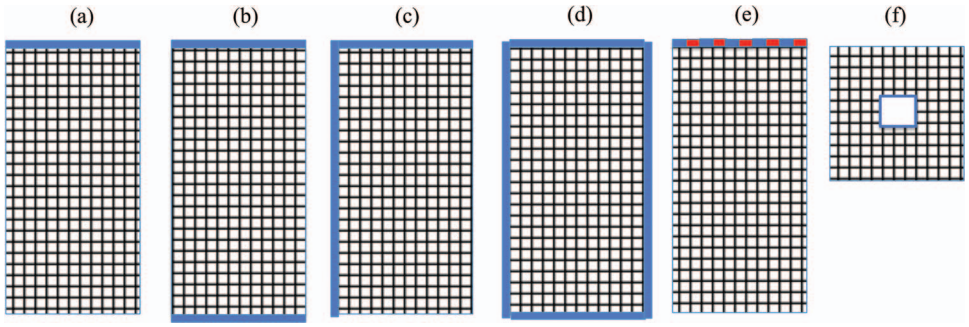

FIG. 3. Schematic showing the placement of surface energetics (thick lines) in the six examples presented in this paper. (a) Uniform energetics on a single wall, (b) uniform energetics on opposite walls, (c) uniform energetics on adjacent walls, (d) uniform energetics on all four walls, (e) alternating energetics on a single wall, with the relative energetics being 1:0.6, and (f) uniform energetics on an object in the center of the lattice and neutral energetics on the walls of the lattice. For (f), transitions through the walls of the object in the center were not allowed. Recall that these rectangles and the energetics on the walls extend (project) infinitely above and below the plane of the paper page.

IV. RESULTS AND DISCUSSION

Figure 4(a) is a plot of the fraction of surface contacts computed from Eq. (16), using the largest eigenvalue. Excluding the case of the energetic striping (Fig. 3(e)), the shapes of the four remaining curves seem similar. Some differences exist, as can be seen in Fig. 4(b), where the deviation between the curves as a function of $-\varepsilon/k_BT$ is plotted. Note that the case of opposite walls is nearly identical to the single wall, but it seems apparent that the effect of energetics on adjacent walls changes the shape somewhat. This is due to the added attractive energy near the corner sites, which will become readily apparent when we plot the density of chain segments as a function of $-\varepsilon/k_BT$. It is also apparent that energetic striping not only significantly changes the shape of the curve, but also shifts the phase transition to lower temperatures, i.e., higher $-\varepsilon/k_BT$. This point will be examined in more depth, later in this paper.

Figure 5 contains contour plots computed using Eq. (15) of the normalized chain segment density probability on the defined x-y lattice at temperatures above the phase transition, during the phase transition, and after the phase transition. The first thing that can be seen from the $-\varepsilon/k_BT = 0$ cases (top row) is that chain segment density is effectively zero near the surfaces and the effect of segment exclusion is even greater at the corners due to the far larger reduction in the number of configurations that would be available to the polymer chains in those regions. The "corner effect" is clear even after the phase transition, i.e., surface adsorption. In those cases where the adjacent wall has neutral energetics, the highest chain segment density is near the center of the wall and drops off to zero near the corners, as can be seen in Figs. 5(a) and 5(b). In cases where the adjacent walls have equally attractive surfaces, adsorption will occur at the corners, but only at very high $-\varepsilon/k_BT$, as can be seen in Figs. 5(c) and 5(d). As mentioned previously, this explains the differences in the phase transition shape shown in Fig. 4(b).

The use of this matrix method on lattices such as those shown in Figs. 3(a)–3(d) shows largely what is intuitively expected from polymer physics. The true power of the lattice technique really comes out when considering lattices such as Figs. 3(e) and 3(f) or more intricate extensions of these

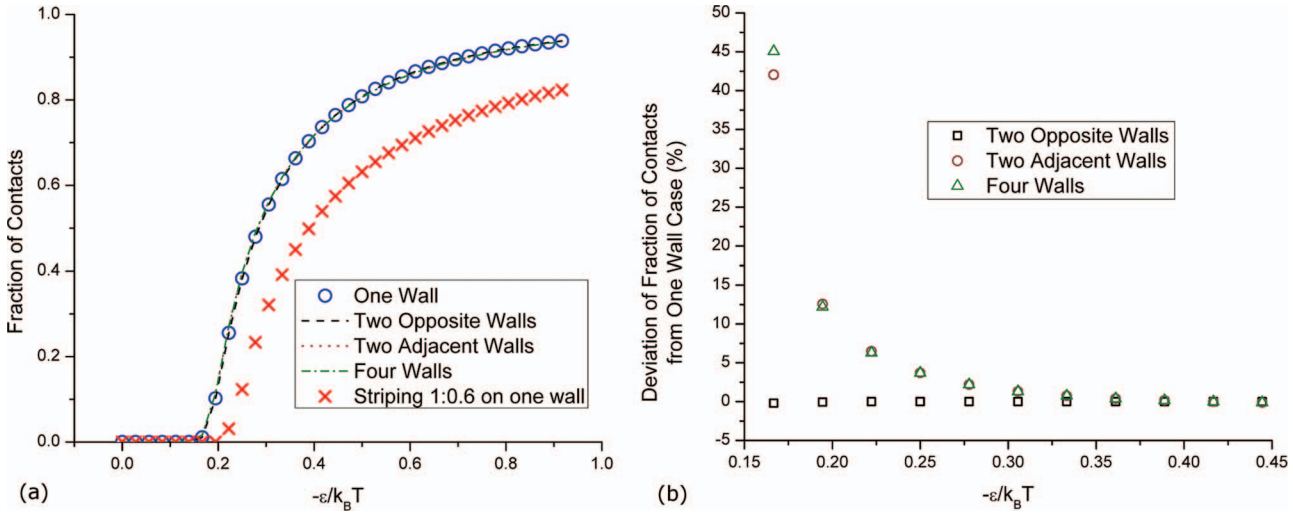

FIG. 4. (a) Fraction of surface contacts as a function of $-\varepsilon/k_BT$, computed from the largest eigenvalue for a 100 × 200 ($N_x \times N_y$) lattice, and (b) plot of the deviation of the fraction of contacts from that corresponding to energetics on one wall (note the striping case was excluded from (b) due to the obvious difference in its shape in (a)).

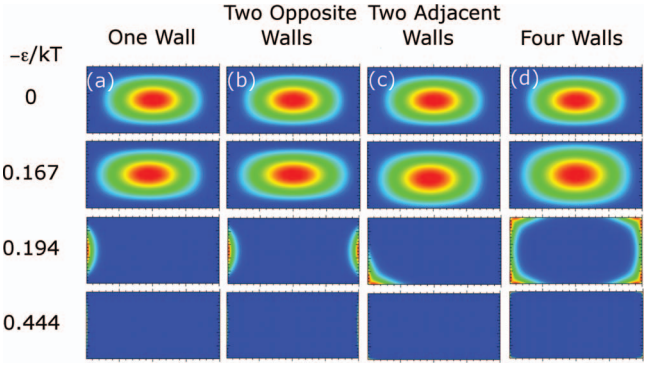

FIG. 5. Density probability contour plots of 100 × 200 lattice ($N_x \times N_y$). Red indicates areas of highest segment density and dark blue indicates areas of zero or nearly zero segment density, (red > orange > yellow > green > cyan > blue). (a)–(d) correspond to the matrices indicated in Figs. 3(a)–3(d), respectively. In each column moving from the top to the bottom corresponds to decreasing temperature (increasing wall attraction) with $-\varepsilon/k_BT = 0, 0.167, 0.194, 0.444$.

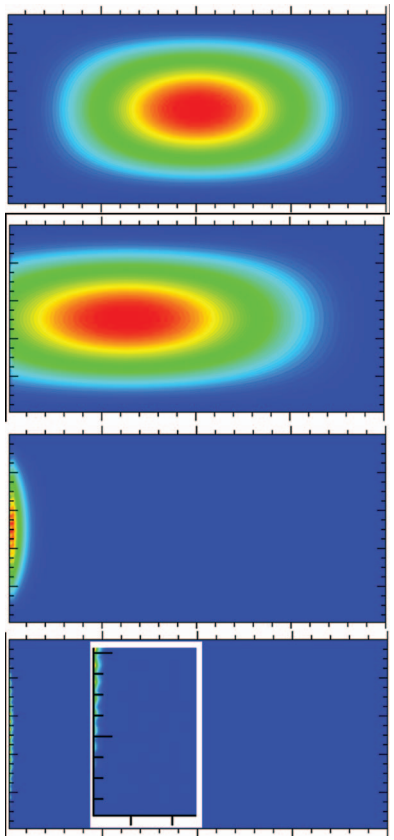

FIG. 6. Density probability contour plots of 100 × 200 lattice ($N_x \times N_y$) for the case of striping of the energetics as shown in Fig. 3(e). Red indicates areas of highest segment density and dark blue indicates areas of zero or nearly zero segment density (red > orange > yellow > green > cyan > blue). Starting at the top of the figure, the plots correspond to decreasing temperature (increasing wall attraction), of $-\varepsilon/k_BT = 0, 0.222, 0.250, 0.444$. Note that the middle two values of $-\varepsilon/k_BT$ differ from those in Fig. 5 due to the shift in the phase transition. The inset in the bottom contour plot is an enlarged version of the bottom left hand corner ($-\varepsilon/k_BT = 0.444$) to show the structure of density due to the striping.

lattices, which are difficult,[26–28] if not impossible, to treat using continuum methods. As shown previously in the case of striping, i.e., non-uniform surface chemistry, a shift in the phase transition temperature (critical condition) ($-\varepsilon/k_BT$) occurs. This result is of immediate importance to the field of polymer chromatography, as it tells us that if the surface chemistry is not uniform then the binding strength must be larger to cause adsorption of the polymer molecules. Figure 4(a) shows that the fraction of segments on the surface is less than the case of uniform energetics, i.e., 0.82 versus 0.94 (for $-\varepsilon/k_BT = 0.944$), respectively. Through the use of the density plot, Fig. 6, we can explore the nature of this effect. In the plot for $-\varepsilon/k_BT = 0.444$ (bottom plot), it is clear that the energetic striping is causing structuring in the surface density (see inset). In the next paper in this series, we will examine this effect as a function of chain length.

In addition to varying the surface energies, we can define structures in the lattice. These structures could either be on the walls of the lattice, such as exploring the effects of surface roughness, or creating a specifically shaped object in the center of the lattice with unique site-specific energetics as would be useful in examining protein binding. A coaxial geometry, shown in Fig. 3(f), was treated as an example. (Recall that unrestrained motion in the z-axis is allowed, so we are examining an infinite rectangular cylinder. The object in the center that looks like a box is effectively a smaller infinite rectangular cylinder centered in the middle of the lattice.)

During the phase transition (see Fig. 7), the outside corners of the object end up with the highest segment density, due to the increased number of configurations relative to the surfaces of the object as contrasted with its inverse, the "corner effect," we mentioned previously. A slight modification to the size/placement of this object reveals a size dependent phenomenon. In Fig. 8, the object's size is reduced by one

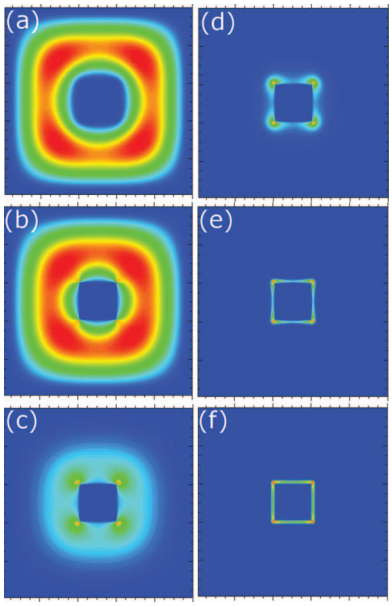

FIG. 7. Density probability contour plots of 100 × 100 lattices ($N_x \times N_y$) with rectangular 21 × 21 objects in the center with uniform energetics on all sides of the object. The surface energetics vary as $-\varepsilon/k_BT =$ (a) 0, (b) 0.139, (c) 0.167, (d) 0.194, (e) 0.444, and (f) 0.944.

lattice row and column each in the x and y dimensions, without moving the position of the lower left hand corner of the object. This provides just slightly more room in the upper right hand corner of lattice, inducing a quite prominent effect at the highest temperatures (Figs. 8(a) and 8(b), lowest $-\varepsilon/k_BT$). After the phase transition, the effect disappears when the attraction of the surfaces becomes the dominating force (Figs. 8(d)–8(f)). This shows that this technique has the capability to examine finite size effects, as would be relevant, for example, to the case of confined films or polymer chains tethered to nanoparticles as the particles get closer together.

Thus far these lattices have shown clear finite size effects; however, it is possible to remove some of the constraints, and thus some finite size effects, without increasing the size of the lattice. In the infinite chain limit, examined here, the chain can explore all space within the lattice. As such, under certain circumstances, periodic boundary conditions can be employed on the "neutral" walls such that the "corner" and finite size effects described above can be eliminated or minimized, by including some additional matrix elements that allow for transitions between the lattice sites on the neutral walls. For example, referring once more to the lattice of Fig. 1, transitions can be allowed between lattice sites 1 and 11 (by adding w_{11} at row 1, column 11 and w_1 at row 11, column 1 in the matrix of Fig. 2), lattice sites 2 and 12 (by adding w_{12} at row 2, column 12 and w_2 at row 12, column 2 in the matrix of Fig. 2), etc.

Figures 9(a) and 9(b) show density probability contours for the lattices of Fig. 3(b) (at $-\varepsilon/k_BT = 0$) and Fig. 3(e) (for $-\varepsilon/k_BT = 0.250$), respectively, where periodic boundaries have been placed on the top and bottom neutral walls. Figures 9(c) and 9(d) show equivalent plots to Figs. 7(a) and 8(a) for the symmetric and asymmetric objects in the center of the lattice but with transitions now allowed between the top and bottom and left and right neutral walls. The shapes of the density contours are exactly as would be expected from the removal of the corner and wall constraints, as seen in Figs. 9(a) and 9(b). The strong effect of the asymmetry of the object has almost been eliminated, as can be seen by comparing plots in Figs. 9(c) and 9(d). The differences are primarily a scale effect – such that the plot is "zoomed" in more on the larger (21 × 21) object. Hence, when one is interested solely in the adsorption behavior on a structured surface, the surface size (number of lattice sites) need be made only large enough to adequately describe the repeating period in the surface, thus reducing the total size of the matrix, and hence the computation time.

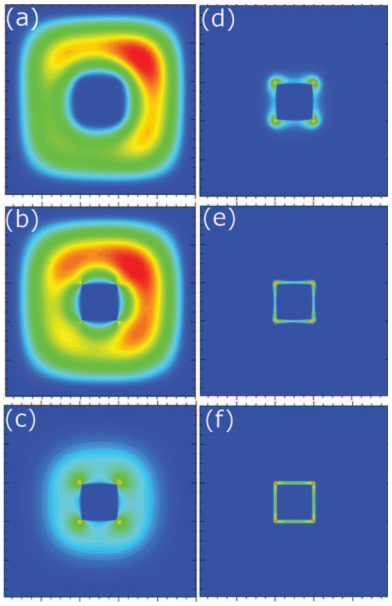

FIG. 8. Density probability contour plots of 100 × 100 lattices ($N_x \times N_y$) with rectangular 20 × 20 slightly off-centered objects with uniform energetics on all sides of the object. The surface energetics vary as $-\varepsilon/k_BT$ = (a) 0, (b) 0.139, (c) 0.167, (d) 0.194, (e) 0.444, and (f) 0.944.

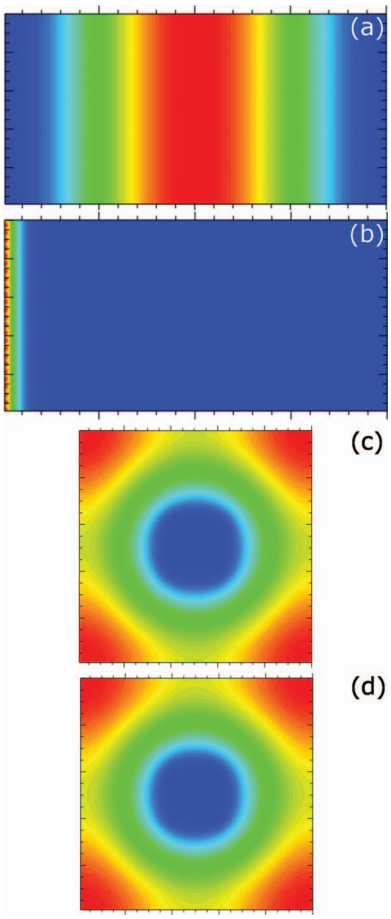

FIG. 9. Density probability contour plots employing periodic boundary conditions as described in the text. (a) Lattice of Fig. 3(b) (at $-\varepsilon/k_BT = 0$) connecting top and bottom walls; (b) lattice of Fig. 3(e) (for $-\varepsilon/k_BT = 0.250$) connecting top and bottom walls; (c) lattice of Fig. 3(f) (at $-\varepsilon/k_BT = 0$) with 20 × 20 object and connecting top and bottom and left and right walls; and (d) lattice of Fig. 3(f) (at $-\varepsilon/k_BT = 0$) with 21 × 21 object and connecting top and bottom and left and right walls.

To demonstrate the validity and usefulness of combining surface energy structuring and periodic boundary conditions, we chose to examine a structure similar to the one studied by Seok *et al.*,[26] who used an analytical density functional theory of alternating stripes of attractive and repulsive energetics as a function of stripe width. Because of the shift in phase transition observed for the striping case studied earlier in this paper, we first examined the location of the phase transition (critical condition for adsorption $-\varepsilon_c/k_BT$) as a

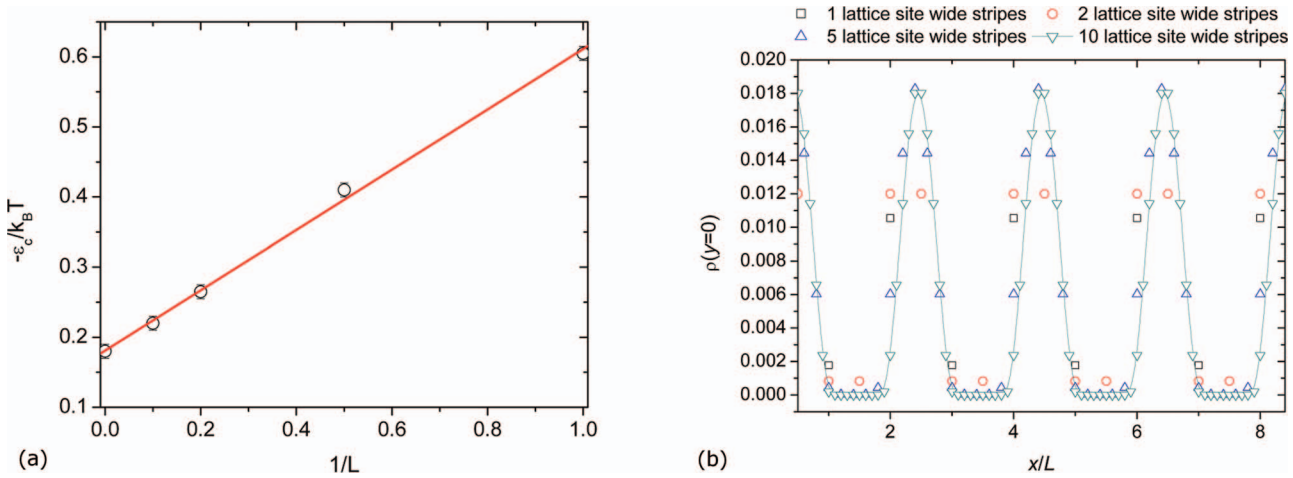

FIG. 10. (a) Critical condition for adsorption $(-\varepsilon_c/k_BT)$ as a function of inverse stripe width $(1/L)$ for stripes with alternating attractive and repulsive energetics computed on a 100 × 100 lattice. (b) Surface density $[\rho(y = 0)]$ at a reduced adsorption energy of $(-\varepsilon/k_BT)/(-\varepsilon_c/k_BT) = 0.25$ versus surface position (x) normalized against stripe width for stripe widths $L = 1, 2, 5$, and 10 lattice sites.

function of the width of the stripe. Figure 10(a) shows the result, which appears to be a nearly linear relationship between the location of the phase transition and the inverse stripe width for stripes ranging from a lattice width of 1 to an infinite lattice width, i.e., uniform surface coverage. The limiting value for the critical condition at $1/L = 0$ is equal to 0.18, which is approximately equivalent to the expected value of ln(6/5) derived analytically by the original DiMarzio-Rubin pseudo 3D matrix method.[2,6] The linearity of the plot suggests an underlying scaling relationship for the phase transition that could be useful in analyzing the effect of surface heterogeneities for polymer chromatography. This dependence of the critical condition on the stripe width indicates that a proper comparison of the surface density as a function of stripe width must be performed by examining the density profiles at a reduced adsorption energy[2] defined as $(-\varepsilon/k_BT)/(-\varepsilon_c/k_BT)$.

Figure 10(b) shows the surface density as a function of position on the surface normalized against the stripe width for a reduced adsorption energy of 0.25. The datasets show reasonable agreement, with the largest deviation being at $L = 1$. The results show qualitative agreement with the shapes of curves in the work of Seok *et al.* The main differences are the sharpness of the density peaks on the attractive stripes. We attribute this to the fact that we are not accounting for excluded volume in the current method and thus far higher surface densities are possible, although as we have mentioned self-consistent approaches are possible with the matrix method.

V. CONCLUSIONS

The power of matrix methods was already well established when they were limited to uniform surface energies, and we have extended it to higher dimensions to enable examination of a myriad of problems of a polymer at an interface. The flexibility of this exact method for treating energy gradients, arbitrarily shaped surfaces, arbitrarily shaped objects, and dimensionalities beyond the pseudo-three-dimensional case of the original Di Marzio-Rubin model, has been demonstrated. We have also identified some phenomena that bear further examination. The case of uneven surface energies (striping) was shown to cause a shift in the phase transition temperature (critical condition) and changes in the shape of the curve, which will have real relevance and is of great importance to polymer chromatography. We have also shown the capability of this technique to examine finite size effects caused by asymmetries that will be present in nearly any system, i.e., at small enough regions of confinement the motion of objects will result in asymmetries in the amount of space available to the polymer chain. While in this case we cannot examine the dynamics, we can examine the equilibrium solutions corresponding to the different states. In the next paper in this series, we will expand upon the theoretical framework for the case of finite chain length. The method described in this paper in many ways lies between continuum approaches and Monte Carlo methods, as it can rapidly provide equilibrium solutions while enabling easy definition of boundary conditions. The advantages to our expanded method are: (1) finite length polymers are treated easily, in contrast to the Gaussian approximation, which only works for large molar masses. Thus, it is complementary to, rather than in competition with, the Gaussian approximation. (2) Copolymers can be treated easily because the monomer attraction to the lattice site is monomer specific as well as lattice site specific. This feature will be useful for biopolymers as well as synthetic polymers. (3) The structure of the monomers can be modeled to mimic actual chemical monomer structure. This circumvents the "resolution limitation" of the Gaussian (continuum) approximation.[16] While not presented in this work, we can write matrices for straight line monomers of k sites thereby having a Kuhn-like approach to the problem. The ultimate aim is to model a chemical monomer as a specific arrangement of k monomers, which we can chain together to form a realistic polymer. (4) The surface can be made both chemically inhomogeneous as well as physically inhomogeneous. This allows for stereospecific interaction simultaneously with chemically specific interaction. We have already discussed the relevance of this concept to chromatography. This "hand and glove"

approach to molecular interaction has obvious biological and catalysis implications.

As a final note, we point out that our work has applications beyond those to polymers. The method presented in this paper is also a solution to the diffusion equation. As such, polymer chain length can be replaced by time, and diffusion can be studied on a lattice with a temporally evolving structure or in a time-dependent chemical or electrical field. More formally, the equation describing the diffusion of particles in a spatially varying field V is, according to Kac,[29] given by

$$\frac{\partial \Psi}{\partial t} = D\nabla^2\Psi - \frac{V}{k_B T}\Psi. \tag{17}$$

If we allow t to be proportional to monomer number as we create the polymer chain, then we see that our work describes the Green's function of Ψ. An improvement over the Kac equation is that our Green's function describes the case when V is a function of both position and time. This is because our energies w_j are monomer specific.

ACKNOWLEDGMENTS

This work is an official contribution of the National Institute of Standards and Technology; it is not subject to copyright in the United States.

APPENDIX A: DERIVATION OF THE DENSITY RELATIONSHIP

The notation and the beginning of the derivation in this appendix are taken closely from the paper by Di Marzio and Rubin. However, it is extended (1) to arbitrary dimensions and (2) to allow for site-specific affinities throughout the matrix. Additionally, since Eq. (3) is used in this paper instead of Eq. (5), the order of many of the variables will be different.

If $\mathbf{P}(N)^{\mathrm{T}}$ is the probability vector describing the probability of being at each lattice site after N steps, then it can be defined as

$$\mathbf{P}(N)^{\mathrm{T}} = \mathbf{P}(0)^{\mathrm{T}}\mathbf{W}^N. \tag{A1}$$

From this equation, the normalization sum (or equivalently the partition function Q) is computed as [P(N)U]. We can then re-write Eq. (12), the normalized probability of finding a segment at lattice site m, as

$$\rho_m = \frac{\frac{d}{d\theta_m}\left[\mathbf{P}(N)^{\mathrm{T}}\mathbf{U}\right]\big|_{\theta_m=0}}{\mathbf{P}(N)^{\mathrm{T}}\mathbf{U}} \tag{A2}$$

and

$$\begin{aligned}\frac{d}{d\theta_m}[\mathbf{P}(N)^{\mathrm{T}}\mathbf{U}]\bigg|_{\theta_m=0} &= \sum_{n=1}^{N}\mathbf{P}(n-1)^{\mathrm{T}}\left.\frac{d\mathbf{W}}{d\theta_m}\right|_{\theta_m}\mathbf{W}^{N-n}\mathbf{U} \\ &= \sum_{n=1}^{N}\mathbf{P}(0)^{\mathrm{T}}\mathbf{W}^{n-1}\left.\frac{d\mathbf{W}}{d\theta_m}\right|_{\theta_m}\mathbf{W}^{N-n}\mathbf{U}.\end{aligned} \tag{A3}$$

λ_j is the jth eigenvalue of the matrix $\mathbf{W}$, with corresponding left and right eigenvectors $\mathbf{l}_j$ and $\mathbf{r}_j$, respectively, which means by definition that

$$\mathbf{l}_j\mathbf{W} = \lambda_j\mathbf{l}_j, \tag{A4}$$

$$\mathbf{W}\mathbf{r}_j = \lambda_j\mathbf{r}_j. \tag{A5}$$

It follows readily from vector mathematics that we can rewrite both $\mathbf{P}(0)$ and $\mathbf{U}$ in terms of the eigenvectors. We define $\mathbf{U}$ as

$$\mathbf{U} = \sum_{j=1}^{M} c_j\mathbf{r}_j, \tag{A6}$$

and multiply both sides by $\mathbf{l}_j$

$$\mathbf{l}_j\cdot\mathbf{U} = \mathbf{l}_j\cdot\sum_{j=1}^{M} c_j\mathbf{r}_j, \tag{A7}$$

but recall that for eigenvectors

$$\mathbf{l}_i\mathbf{r}_j = 0 \text{ for } i \neq j. \tag{A8}$$

Thus, Eq. (A6) is only valid when

$$c_j = \frac{\mathbf{l}_j\cdot\mathbf{U}}{\mathbf{l}_j\cdot\mathbf{r}_j} = \frac{1}{\mathbf{l}_j\cdot\mathbf{r}_j}\sum_{k=1}^{M} l_j(k). \tag{A9}$$

Similarly, $\mathbf{P}(0)^{\mathrm{T}}$ can be given by

$$\mathbf{P}(0)^{\mathrm{T}} = \sum_{i=1}^{M} d_i\mathbf{l}_i, \tag{A10}$$

when

$$d_j = \frac{\mathbf{P}(0)^{\mathrm{T}}\cdot\mathbf{r}_j}{\mathbf{l}_j\cdot\mathbf{r}_j}. \tag{A11}$$

Then by substituting Eqs. (A6) and (A10) into Eq. (A3), we obtain

$$\frac{d}{d\theta_m}\left[\mathbf{P}(N)^{\mathrm{T}}\mathbf{U}\right]\big|_{\theta_m=0} = \sum_{i,j,n} d_j\mathbf{l}_j\ \mathbf{W}^{n-1}\left.\frac{d\mathbf{W}}{d\theta_m}\right|_{\theta_m}\mathbf{W}^{N-n}c_i\mathbf{r}_i. \tag{A12}$$

Using Eqs. (A4) and (A5) $(n-1)$ and $(N-n)$ times each, respectively, yields

$$\begin{aligned}\frac{d}{d\theta_m}\left[\mathbf{P}(N)^{\mathrm{T}}\mathbf{U}\right]\big|_{\theta_m=0} &= \sum_{i,j,n} d_j\mathbf{l}_j\ \lambda_j^{n-1}\left.\frac{d\mathbf{W}}{d\theta_m}\right|_{\theta_m}\lambda_i^{N-n}c_i\mathbf{r}_i \\ &= \sum_{i,j,n} d_j\lambda_j^{n-1}\left[\mathbf{l}_j\left.\frac{d\mathbf{W}}{d\theta_m}\right|_{\theta_m=0}\mathbf{r}_i\right]\lambda_i^{N-n}c_i.\end{aligned} \tag{A13}$$

Excluding the fact that we have used Eq. (3) instead of Eq. (5), and the implications thereof, we have closely followed the approach of Di Marzio and Rubin to this point, however, due to the additional energetics of the lattice and higher dimensionalities, we will now deviate from it. For the pseudo four-dimensional cubic lattice, it can easily be shown

that away from corners and edges of the lattice:

$$\left.\frac{d\mathbf{W}}{d\theta_m}\right|_{\theta_m=0} = \begin{bmatrix} \vdots & \vdots \\ & (w_m)_{m-N_y-N_x,m} \\ & \vdots \\ & (w_m)_{m-N_y,m} \\ & \vdots \\ 0 \cdots\cdots\cdots\cdots & (w_m)_{m-1,m} \quad (s_0 w_m)_{m,m} \quad \cdots\cdots\cdots\cdots 0 \\ & (w_m)_{m+1,m} \\ & \vdots \\ & (w_m)_{m+N_y,m} \\ & \vdots \\ & (w_m)_{m+N_y+N_x,m} \\ & \vdots \end{bmatrix}_{(N_x\times N_y\times N_z),(N_x\times N_y\times N_z)}$$

where "…" in above matrix means all zeros and w_{m} is the weighting factor defined earlier. Multiplication on the left by $\mathbf{l}_j$ and on the right by $\mathbf{r}_i$ yields

$$\begin{aligned}&\mathbf{l}_j \left.\frac{d\mathbf{W}}{d\theta_m}\right|_{\theta_m=0} \mathbf{r}_i \\ &= (l_{j,m-N_y-N_x} + l_{j,m-N_y} + l_{j,m-1} + l_{j,m}s_0 + l_{j,m+1} \\ &\quad + l_{j,m+N_y} + l_{j,m+N_y+N_x}) w_m r_{i,m}. \end{aligned} \tag{A14}$$

For corners and edges, terms that are unphysical are removed, i.e., at a lattice site on a wall, there are no sites defined on the other side of the wall, only nearest neighbor sites are retained. If we now substitute Eq. (A14) into Eq. (A13), it yields the following:

$$\begin{aligned}&\frac{d}{d\theta_m}\left[\mathbf{P}(N)^{\mathrm{T}}\mathbf{U}\right]\Big|_{\theta_m=0} \\ &= \sum_{i,j,n} d_j \lambda_j^{n-1} [(l_{j,m-N_y-N_x} + l_{j,m-N_y} + l_{j,m-1} + l_{j,m}s_0 \\ &\quad + l_{j,m+1} + l_{j,m+N_y} + l_{j,m+N_y+N_x}) r_{i,m} w_m] \lambda_i^{N-n} c_i. \end{aligned} \tag{A15}$$

For sufficiently large N, the maximum eigenvalue, designated by a subscript 0, will dominate, and we can, therefore, write

$$\begin{aligned}&\frac{d}{d\theta_m}\left[\mathbf{P}(N)^{\mathrm{T}}\mathbf{U}\right]\Big|_{\theta_m=0} \\ &= d_0 \lambda_0^{N-1} [(l_{0,m-N_y-N_x} + l_{0,m-N_y} + l_{0,m-1} + l_{0,m}s_0 \\ &\quad + l_{0,m+1} + l_{0,m+N_y} + l_{0,m+N_y+N_x}) r_{0,m} w_m] c_0. \end{aligned} \tag{A16}$$

The normalization sum $[\mathbf{P}(N)^{\mathrm{T}}\mathbf{U}]$ can be written directly as

$$\begin{aligned}\mathbf{P}(N)^T\mathbf{U} &= \left[\sum_{j=1}^{M} d_j \mathbf{l}_j\right] \mathbf{W}^N \left[\sum_{j=1}^{M} c_j \mathbf{r}_j\right] \\ &= \left[\sum_{j=1}^{M} d_j \lambda_j^N \mathbf{l}_j\right] \left[\sum_{j=1}^{M} c_j \mathbf{r}_j\right] \\ &= \sum_{j=1}^{M} d_j \lambda_j^N c_j \mathbf{l}_j \mathbf{r}_j \\ &= d_0 \lambda_0^N c_0 \mathbf{l}_0 \mathbf{r}_0, \end{aligned} \tag{A17}$$

where again only the maximum eigenvalue has been retained in the final summation. Substitution of Eqs. (A16) and (A17)

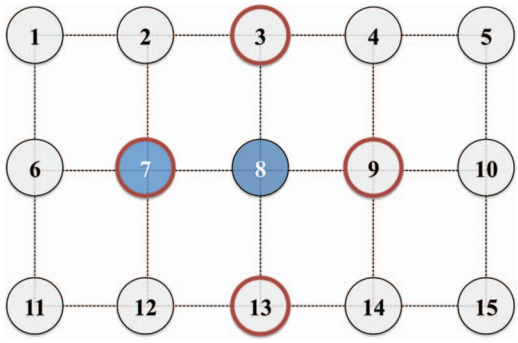

FIG. 11. Schematic of Fig. 1, showing possible moves for a chain starting at lattice site 7 and passing through lattice site 8. The sites marked with bold red lines are the possible ending sites.

into Eq. (A2) and simplifying yields

$$\rho_m = \frac{\left[\left(\sum_{i=\text{nearest neighbors to } m} l_{0,i}\right) + s_0 l_{0,m}\right] r_{0,m} w_m}{\lambda_0 \mathbf{l}_0 \mathbf{r}_0}. \quad \text{(A18)}$$

By examining this derivation, it is now clear that the above equation is generalized to any dimensionality or lattice coordination.

APPENDIX B: EXAMPLE OF A CHAIN WALKING ON THE LATTICE OF FIG. 1

Consider the following example, the case of a polymer chain with N monomers starting at position 7 on the lattice of Fig. 1 and ending at lattice site j. In this case, we begin with Eq. (3), with $k = 7$, i.e.,

$$Q = (\mathbf{P}(..0..w_j..0..))^T \mathbf{W}^{N-1} \mathbf{U}_{k=7},$$

then $\mathbf{W}^{N-1}\mathbf{U}_{k=7}$ is given for the 2d lattice of Fig. 1 as

$$\mathbf{W}^{N-1}\mathbf{U}_{k=7} = \begin{bmatrix}
0 & w_2 & 0 & 0 & 0 & w_6 & 0 & 0 & 0 & 0 & 0 & 0 & 0 & 0 & 0 \\
w_1 & 0 & w_3 & 0 & 0 & 0 & w_7 & 0 & 0 & 0 & 0 & 0 & 0 & 0 & 0 \\
0 & w_2 & 0 & w_4 & 0 & 0 & 0 & w_8 & 0 & 0 & 0 & 0 & 0 & 0 & 0 \\
0 & 0 & w_3 & 0 & w_5 & 0 & 0 & 0 & w_9 & 0 & 0 & 0 & 0 & 0 & 0 \\
0 & 0 & 0 & w_4 & 0 & 0 & 0 & 0 & 0 & w_{10} & 0 & 0 & 0 & 0 & 0 \\
w_1 & 0 & 0 & 0 & 0 & 0 & w_7 & 0 & 0 & 0 & w_{11} & 0 & 0 & 0 & 0 \\
0 & w_2 & 0 & 0 & 0 & w_6 & 0 & w_8 & 0 & 0 & 0 & w_{12} & 0 & 0 & 0 \\
0 & 0 & w_3 & 0 & 0 & 0 & w_7 & 0 & w_9 & 0 & 0 & 0 & w_{13} & 0 & 0 \\
0 & 0 & 0 & w_4 & 0 & 0 & 0 & w_8 & 0 & w_{10} & 0 & 0 & 0 & w_{14} & 0 \\
0 & 0 & 0 & 0 & w_5 & 0 & 0 & 0 & w_9 & 0 & 0 & 0 & 0 & 0 & w_{15} \\
0 & 0 & 0 & 0 & 0 & w_6 & 0 & 0 & 0 & 0 & 0 & w_{12} & 0 & 0 & 0 \\
0 & 0 & 0 & 0 & 0 & 0 & w_7 & 0 & 0 & 0 & w_{11} & 0 & w_{13} & 0 & 0 \\
0 & 0 & 0 & 0 & 0 & 0 & 0 & w_8 & 0 & 0 & 0 & w_{12} & 0 & w_{14} & 0 \\
0 & 0 & 0 & 0 & 0 & 0 & 0 & 0 & w_9 & 0 & 0 & 0 & w_{13} & 0 & w_{15} \\
0 & 0 & 0 & 0 & 0 & 0 & 0 & 0 & 0 & w_{10} & 0 & 0 & 0 & w_{14} & 0
\end{bmatrix}^{N-1} \begin{bmatrix} 0 \\ 0 \\ 0 \\ 0 \\ 0 \\ 0 \\ 1 \\ 0 \\ 0 \\ 0 \\ 0 \\ 0 \\ 0 \\ 0 \\ 0 \end{bmatrix} = \mathbf{W}^{N-2} \begin{bmatrix} 0 \\ w_7 \\ 0 \\ 0 \\ 0 \\ w_7 \\ 0 \\ w_7 \\ 0 \\ 0 \\ 0 \\ w_7 \\ 0 \\ 0 \\ 0 \end{bmatrix}$$

the vector on the right hand side can be written as a sum of individual vectors, i.e.,

$$\mathbf{W}^{N-1}\mathbf{U}_{k=7} = \mathbf{W}^{N-2} \begin{bmatrix} 0 \\ w_7 \\ 0 \\ 0 \\ 0 \\ 0 \\ 0 \\ 0 \\ 0 \\ 0 \\ 0 \\ 0 \\ 0 \\ 0 \\ 0 \end{bmatrix} + \mathbf{W}^{N-2} \begin{bmatrix} 0 \\ 0 \\ 0 \\ 0 \\ 0 \\ w_7 \\ 0 \\ 0 \\ 0 \\ 0 \\ 0 \\ 0 \\ 0 \\ 0 \\ 0 \end{bmatrix} + \mathbf{W}^{N-2} \begin{bmatrix} 0 \\ 0 \\ 0 \\ 0 \\ 0 \\ 0 \\ 0 \\ w_7 \\ 0 \\ 0 \\ 0 \\ 0 \\ 0 \\ 0 \\ 0 \end{bmatrix} + \mathbf{W}^{N-2} \begin{bmatrix} 0 \\ 0 \\ 0 \\ 0 \\ 0 \\ 0 \\ 0 \\ 0 \\ 0 \\ 0 \\ 0 \\ 0 \\ w_7 \\ 0 \\ 0 \\ 0 \end{bmatrix}$$

and with one more multiplication by **W** we get

$$\mathbf{W}^{N-1}\mathbf{U}_{k=7} = \mathbf{W}^{N-3}\begin{bmatrix} w_7w_2 \\ 0 \\ w_7w_2 \\ 0 \\ 0 \\ 0 \\ w_7w_2 \\ 0 \\ 0 \\ 0 \\ 0 \\ 0 \\ 0 \\ 0 \\ 0 \end{bmatrix} + \mathbf{W}^{N-3}\begin{bmatrix} w_7w_6 \\ 0 \\ 0 \\ 0 \\ 0 \\ 0 \\ w_7w_6 \\ 0 \\ 0 \\ 0 \\ w_7w_6 \\ 0 \\ 0 \\ 0 \\ 0 \end{bmatrix} + \mathbf{W}^{N-3}\begin{bmatrix} 0 \\ 0 \\ w_7w_8 \\ 0 \\ 0 \\ 0 \\ w_7w_8 \\ 0 \\ w_7w_8 \\ 0 \\ 0 \\ 0 \\ w_7w_8 \\ 0 \\ 0 \end{bmatrix} + \mathbf{W}^{N-3}\begin{bmatrix} 0 \\ 0 \\ 0 \\ 0 \\ 0 \\ 0 \\ w_7w_{12} \\ 0 \\ 0 \\ 0 \\ w_7w_{12} \\ 0 \\ w_7w_{12} \\ 0 \\ 0 \end{bmatrix}.$$

The third vector in the summation describes the possible moves starting at lattice site 7 and passing through lattice site 8. This is shown pictorially in Fig. 11, with the sites marked by bold red lines as possible ending sites, i.e., non-zero probabilities. Note that site 7 is one of the possibilities, because we have not accounted for excluded volume.

To finalize our example, we will now compute the partition function for a 3-monomer chain starting at lattice site 7 and ending at lattice site 13. So using the above result, we can write

$$Q = \mathbf{P}(0,\ldots,w_{13},,\ldots,0)^{\mathrm{T}}\mathbf{W}^2\mathbf{U}_{k=7} = \begin{bmatrix} 0 \\ 0 \\ 0 \\ 0 \\ 0 \\ 0 \\ 0 \\ 0 \\ 0 \\ 0 \\ 0 \\ 0 \\ 0 \\ w_{13} \\ 0 \\ 0 \end{bmatrix}^{\mathrm{T}} \mathbf{W}^2\mathbf{U}_{k=7} = \begin{bmatrix} 0 \\ 0 \\ 0 \\ 0 \\ 0 \\ 0 \\ 0 \\ 0 \\ 0 \\ 0 \\ 0 \\ 0 \\ 0 \\ w_{13} \\ 0 \\ 0 \end{bmatrix}^{\mathrm{T}} \left\{ \begin{bmatrix} w_7w_2 \\ 0 \\ w_7w_2 \\ 0 \\ 0 \\ 0_0 \\ w_7w_2 \\ 0 \\ 0 \\ 0 \\ 0 \\ 0 \\ 0 \\ 0 \\ 0 \end{bmatrix} + \begin{bmatrix} w_7w_6 \\ 0 \\ 0 \\ 0 \\ 0 \\ 0 \\ w_7w_6 \\ 0 \\ 0 \\ 0 \\ w_7w_6 \\ 0 \\ 0 \\ 0 \\ 0 \end{bmatrix} + \begin{bmatrix} 0 \\ 0 \\ w_7w_8 \\ 0 \\ 0 \\ 0 \\ w_7w_8 \\ 0 \\ w_7w_8 \\ 0 \\ 0 \\ 0 \\ w_7w_8 \\ 0 \\ 0 \end{bmatrix} + \begin{bmatrix} 0 \\ 0 \\ 0 \\ 0 \\ 0 \\ 0 \\ w_7w_{12} \\ 0 \\ 0 \\ 0 \\ w_7w_{12} \\ 0 \\ w_7w_{12} \\ 0 \\ 0 \end{bmatrix} \right\},$$

which is simply

$$Q = w_7w_8w_{13} + w_7w_{12}w_{13},$$

which is the expected correct answer for a chain starting at site 7 and ending at site 13 in 2 steps.

[1] K. F. Freed, J. Dudowicz, E. B. Stukalin, and J. F. Douglas, J. Chem. Phys. **133**, 094901 (2010).
[2] L. I. Klushin, A. A. Polotsky, H.-P. Hsu, D. A. Markelov, K. Binder, and A. M. Skvortsov, Phys. Rev. E **87**, 022604 (2013).
[3] M. Muthukumar, in *Advances in Chemical Physics* (John Wiley & Sons, Inc., 2012), pp. 129–196.
[4] E. A. Di Marzio and F. L. McCrackin, J. Chem. Phys. **43**, 539 (1965).
[5] R. J. Rubin, J. Chem. Phys. **43**, 2392 (1965).
[6] E. A. DiMarzio and R. J. Rubin, J. Chem. Phys. **55**, 4318 (1971).
[7] J. M. H. M. Scheutjens and G. J. Fleer, J. Phys. Chem. **83**, 1619 (1979).
[8] J. M. H. M. Scheutjens and G. J. Fleer, J. Phys. Chem. **84**, 178 (1980).
[9] G. H. Fredrickson, *The Equilibrium Theory of Inhomogeneous Polymers* (Oxford University Press, Oxford, 2006).
[10] C. M. Guttman, E. A. Di Marzio, and J. F. Douglas, Macromolecules **29**, 5723 (1996).
[11] E. F. Casassa, J. Polym. Sci. Part B: Polym. Lett. **5**, 773 (1967).
[12] E. F. Casassa and Y. Tagami, Macromolecules **2**, 14 (1969).
[13] E. F. Casassa, J. Phys. Chem. **75**, 3929 (1971).
[14] E. A. Di Marzio, C. M. Guttman, and A. Mah, Macromolecules **28**, 2930 (1995).
[15] I. Park, S. Park, D. Cho, T. Chang, E. Kim, K. Lee, and Y. J. Kim, Macromolecules **36**, 8539 (2003).
[16] A. A. Gorbunov and A. M. Skvortsov, Adv. Colloid Interface Sci. **62**, 31 (1995).
[17] E. A. Di Marzio and C. M. Guttman, e-print arXiv:1110.0142 [physics.gen-Ph] (2011).
[18] Y. Saad, *Sparsekit: A Basic Tool Kit for Sparse Matrix Computations* (Computer Science Department, University of Minnesota, 1994).
[19] Certain commercial equipment, instruments, or materials are identified in this paper in order to specify the experimental procedure accurately. Such

identification is not intended to imply recommendation or endorsement by the National Institute of Standards and Technology, nor is it intended to imply that the materials or equipment identified are necessarily the best available for the purpose.
[20]See http://www.caam.rice.edu/software/ARPACK/ for *ARPACK*.
[21]R. B. Lehoucq, D. C. Sorensen, and C. Yang, *ARPACK Users' Guide: Solution of Large-Scale Eigenvalue Problems with Implicitly Restarted Arnoldi Methods* (SIAM, Philadelphia, 1998).
[22]D. Sorensen, SIAM. J. Matrix Anal. Appl. **13**, 357 (1992).
[23]See http://www.netlib/BLAS/ for *BLAS (Basic Linear Algebra Subprograms)*.
[24]W. H. Press, S. A. Teukolsky, W. T. Vetterling, and B. P. Flannery, *Numerical Recipes in Fortran 77: The Art of Scientific Computing*, 2nd ed. (Cambridge University Press, New York, 1992).
[25]See http://plplot.sourceforge.net for *PLplot*.
[26]C. Seok, K. F. Freed, and I. Szleifer, J. Chem. Phys. **112**, 6443 (2000).
[27]A. I. Chervanyov and G. Heinrich, J. Chem. Phys. **125**, 084703 (2006).
[28]A. I. Chervanyov and G. Heinrich, J. Chem. Phys. **129**, 074902 (2008).
[29]M. Kac, Trans. Am. Math. Soc. **65**, 1 (1949).
[30]See supplementary material at http://dx.doi.org/10.1063/1.4857355 for a listing of some of the problems related to polymers at interfaces.